ARMY RESEARCH LABORATORY

On the Different Physical Roles of Hysteresis and Intrinsic Oscillations in Resonant Tunneling Structures

Dwight L. Woolard, Felix A. Buot, David L. Rhodes,
Xiaojia Lu, Robert A. Lux and Barry S. Perlman

ARL-TR-1120 August 1996

NOTICES

Disclaimers

The findings in this report are not to be construed as an official Department of the Army position, unless so designated by other authorized documents.

The citation of trade names and names of manufacturers in this report is not to be construed as official Government endorsement or approval of commercial products or services referenced herein.

REPORT DOCUMENTATION PAGE

Form Approved
OMB No. 0704-0188

1. AGENCY USE ONLY *(Leave blank)*	2. REPORT DATE	3. REPORT TYPE AND DATES COVERED
	August 1996	Technical Report

4. TITLE AND SUBTITLE

On the different physical roles of hysteresis and intrinsic oscillations in resonant tunneling structures

5. FUNDING NUMBERS

6. AUTHOR(S)

Dwight L. Woolard, Felix A. Buot,* David.L. Rhodes, Xiaojia Lu, Robert A. Lux, Barry S. Perlman

7. PERFORMING ORGANIZATION NAME(S) AND ADDRESS(ES)
US Army Research Laboratory (ARL)
Physical Sciences Directorate (PSD)
ATTN: AMSRL-PS-EA
Fort Monmouth, NJ 07703-5601

8. PERFORMING ORGANIZATION REPORT NUMBER

ARL-TR-1120

9. SPONSORING/MONITORING AGENCY NAME(S) AND ADDRESS(ES)

10. SPONSORING/MONITORING AGENCY REPORT NUMBER

11. SUPPLEMENTARY NOTES

*Felix Buot is at the Naval Research Laboratory, Washington, DC 20375-5320

12a. DISTRIBUTION/AVAILABILITY STATEMENT

Approved for public release; distribution is unlimited

12b. DISTRIBUTION CODE

13. ABSTRACT *(Maximum 200 words)*

Electronic sources based upon resonant tunneling diodes (RTDs) usually generate power by establishing limit cycles which exchange energy with storage elements in an external biasing circuit; hence, the output power in this type of implementation will always be limited by extrinsic effects. We verify the presence of multiple energy-storage mechanisms solely within the RTD and characterize the interdependencies necessary to induce intrinsic oscillations observed in quantum mechanical simulations. Specifically, we show that a nonlinear "access" resistance and quantum-well inductance is responsible for the hysteresis, "plateaulike" behavior, and bistability associated with the intrinsic current-voltage (I-V) characteristic. Furthermore, a new circuit-level representative which accurately incorporates the nonlinear dependencies into these heretofore "linear" equivalent-circuit elements is used to demonstrate the different roles, as well as the degree of cooperative interplay, of the intrinsic oscillations and hysteresis in determining the overall I-V characteristics of the RTD.

14. SUBJECT TERMS
resonant tunneling, oscillations, bistable, high frequency electronics
equivalent circuit model

15. NUMBER OF PAGES
43

16. PRICE CODE

17. SECURITY CLASSIFICATION OF REPORT	18. SECURITY CLASSIFICATION OF THIS PAGE	19. SECURITY CLASSIFICATION OF ABSTRACT	20. LIMITATION OF ABSTRACT
Unclassified	Unclassified	Unclassified	UL

NSN 7540-01-280-5500

Standard Form 298 (Rev. 2-89)
Prescribed by ANSI Std. 239-18
298-01

CONTENTS

FIGURES

FIGURES (continued)

On The Different Physical Roles of Hysteresis and Intrinsic Oscillations in Resonant Tunneling Structures

Dwight L. Woolard
U.S. Army Research Laboratory, PSD, Fort Monmouth, NJ 07703-5601

Felix A. Buot
Naval Research Laboratory, Washington, D.C. 20375-5320

David L. Rhodes, Xiaojia Lu, Robert A. Lux and Barry S. Perlman
U.S. Army Research Laboratory, PSD, Fort Monmouth, NJ 07703-5601

Abstract

Electronic sources based upon resonant tunneling diodes (RTDs) usually generate power by establishing limit-cycles which exchange energy with storage elements in an external biasing circuit. Hence, the output power in this type of implementation will always be limited by extrinsic effects. This study verifies the presence of multiple energy-storage mechanisms solely within the RTD and characterizes the interdependencies necessary to induce intrinsic oscillations observed in quantum mechanical simulations. Specifically, this work shows that a nonlinear "access" resistance and quantum-well inductance is responsible for the hysteresis, "plateau-like" behavior, and bistability associated with the intrinsic current-voltage (I-V) characteristic. Furthermore, a new circuit-level representation which accurately incorporates the nonlinear dependencies into these heretofore "linear" equivalent-circuit elements is used to demonstrate the different roles, as well as the degree of cooperative interplay, of the intrinsic oscillations and hysteresis in determining the overall I-V characteristics of the RTD.

I. INTRODUCTION

The intrinsically fast process of resonant tunneling through double barrier heterostructures along with the existence of negative differential resistance (NDR) makes these devices attractive as sources for very high frequency electromagnetic energy. While resonant tunneling diodes (RTDs) have been shown to possess rates of response in the terahertz regime [1] and have been implemented as oscillators up to 712 GHz [2], only microwatt levels of power have been achieved above 100 GHz [3]. Thus, a detailed understanding of the fundamental power limitations in RTD-based sources is needed. Previous analysis aimed at optimizing RTD sources may have been limited more by the design approach than by intrinsic factors. This is true because RTDs are traditionally implemented purely as a NDR element with only a single energy storage mechanism (i.e., device capacitance). Hence, the generation of oscillations must be achieved through limit-cycles which exchange energy with storage elements in the external biasing circuit. In this traditional approach, where oscillations are induced extrinsically, the amount of achievable output power will always be limited by external losses (e.g., contact resistance) and low frequency design constraints (i.e., suppression of bias oscillations). Previously, quantum mechanical simulations of a GaAs-AlGaAs RTD structure have shown the potential for self-oscillations up to 6 THz [4]. If the dynamics surrounding these intrinsic phenomena can be fully understood and controlled, RTD sources based on the self-oscillation process should yield milliwatt levels of power in the terahertz regime [5].

The purpose of this paper is to clearly delineate between the physics responsible for the hysteresis and that of the high-frequency oscillations for intrinsic (i.e., those free of external parasitic coupling) RTD structures. To date, analysis of general oscillation phenomenon in RTD-based sources has either ignored the possibility of multiple energy-storage circuit-elements in the intrinsic device [6,7] or applied linear circuit theory to simplified small-signal diode models with constant coefficients [4,8]. This work incorporates the important intrinsic nonlinearity into the equivalent-circuit parameters for the RTD and is analyzed by numerically generating the nonlinear circuit solutions of the time-dependent behavior. As will be shown, when nonlinear dependencies are properly included it is possible to reproduce the hysteresis, oscillation phenomena, and the overall I-V curves obtained from previous quantum mechanical simulations of the intrinsic RTD

structure [9]. Fundamental physical insight into device nonlinearities is required because it will strongly influence the design and optimization of RTD-based high-frequency power sources embedded within biasing circuitry.

II. BACKGROUND THEORY

In general it is difficult to utilize experimentation to directly extract the intrinsic characteristics of RTD structures. For example, while experimental investigations of RTDs routinely report I-V curves which exhibit a characteristic "plateau-like" hysteresis behavior and bistability, there has been previous debate on whether these phenomena are always a result of oscillations induced by the extrinsic circuit or whether the intrinsic nature of the RTD is sometimes responsible [10,11]. Of the two main groups offering an explanation for this I-V behavior, one attributed the entire phenomenon to intrinsic charge bistability [10] and the other interpreted the results as arising from extrinsic biasing effects [11].

In the intrinsic description of the first group [10], charge build-up in the quantum-well during forward biasing acted to maintain the position of the resonant tunneling (RT) states (i.e., relative to the injecting emitter states). This process leads to higher current values (i.e., in comparison in reverse biasing) until the RT states align with low-lying quantized states in the accumulated region of the emitter. At this point, a gradually falling current (i.e., negative-slope plateau) is obtained until the RT states drop below the emitter conduction-band edge. While this *static* analysis accounted for many features exhibited in the time-average I-V characteristic, it fails to address oscillation behavior or to explain the positive-slope plateau regions exhibited by some RTD structures.

Conversely, the second group [11] attributed the entire I-V behavior to extrinsically-induced high-frequency oscillations. Here, a resonance between the RTD capacitance and the lead-wiring inductance is given credit for introducing plateau features upon a loadline (i.e., source-resistance and NDR) induced hysteresis. Theoretical analysis by others [6,7], was subsequently used to show that extrinsic circuit effects could produce many of the features seen in typical I-V curves; however, most of these studies failed to show hysteresis. Moreover, no attempt was made to precisely correlate these equivalent-circuit studies to a specific RTD (i.e., independently extract

device parameters) embedded in a specific biasing circuit. Hence, a completely unique physical explanation for this phenomenon was not achieved.

Some resolution to this controversial issue came later from the many-body Wigner-distribution-function (MBWDF) numerical simulations of Jensen and Buot [9]. Here, time-dependent quantum transport simulations of a particular GaAs-AlGaAs RTD revealed *intrinsic* high-frequency oscillations for applied bias corresponding to the NDR region of operation. Indeed, the presence of intrinsic autonomous oscillations was found which could not be explained using the arguments of the two groups discussed above. These MBWDF simulations possessed two unique aspects lacking from the investigations of the other groups. First, the numerical procedure incorporated time-dependent self-consistent effects for all dc biases. Second, the simulations utilized a longer simulation "box" length which allowed for an accurate description of the charge dynamics in the buffer regions surrounding the actual resonant tunneling structure (RTS). Note, here we denote the RTS as the barrier-well-barrier regions; whereas, the intrinsic RTD includes both the RTS and the surrounding resistive "access" regions. This accurate description of the charge dynamics within the buffer regions had two important benefits; namely, (i) it allowed for the application of the "inflow/ outflow" boundary conditions, and (ii) it provided for a realistic description of the "access" resistance within the buffer regions (which will be shown later to play a crucial role in the overall behavior of the intrinsic RTD).

At this point, it is important to note that the intrinsic oscillations observed in Ref. [9] were not an artificial result of the boundary conditions utilized in the simulations. While the size of the simulation "box" used in their study was small (i.e., 550 A), the "inflow" and "outflow" states were found to be practically decoupled without the ability to produce noticeable artificial reflections at the boundaries. Furthermore, for all cases considered the boundary electric fields were sufficiently small enough (or negligible) that the use of drifted Fermi distribution for the "inflow" state did not noticeably affect the amplitude or frequency of the oscillations [12,13]. Hence, the average I-V characteristic of these one-dimensional (i.e., transverse dimension assumed infinite) simulations, as shown in Fig. 1, support the notion that RTDs of sufficiently large area possess the inherit ability to manifest bistable behavior.

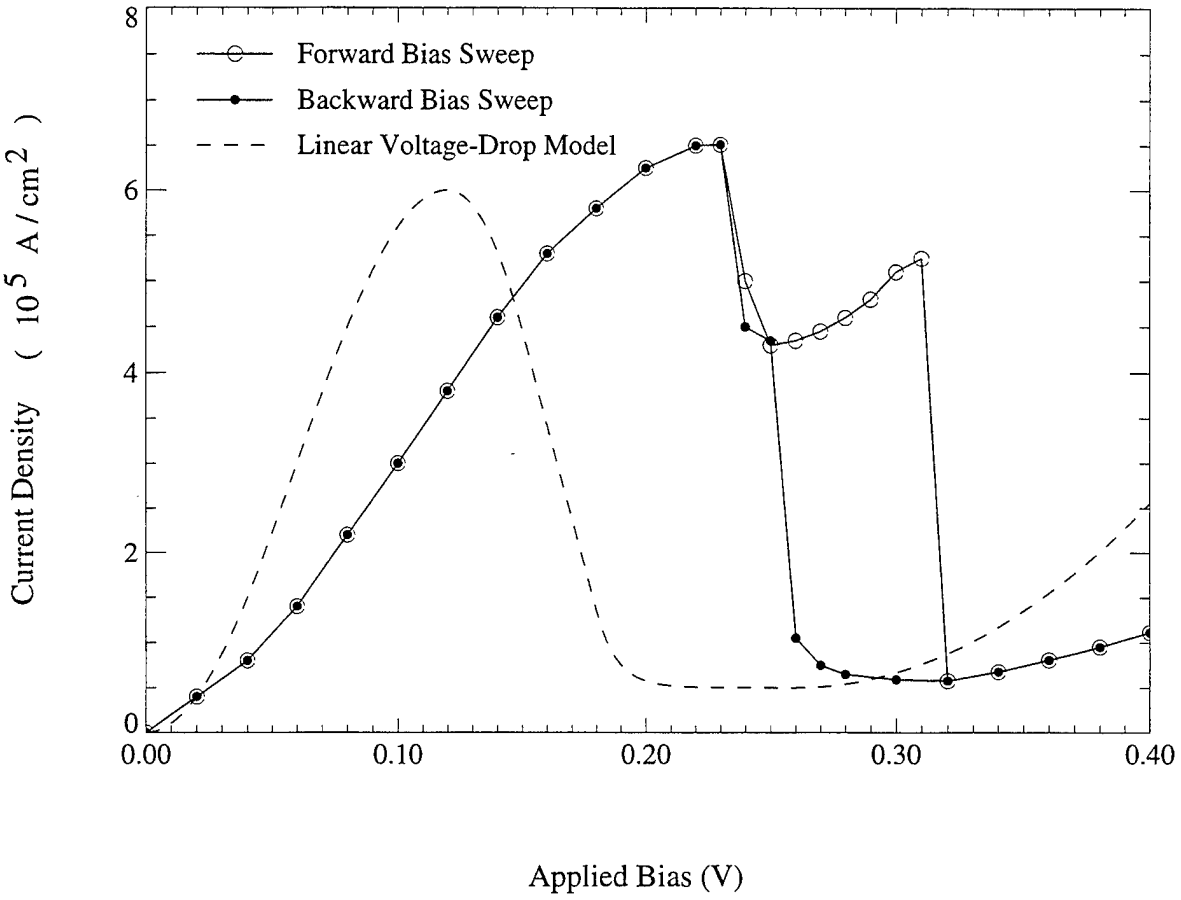

FIG. 1. RTD current density *vs* applied bias from quantum simulations of Ref. 3. Also depicted is the linear voltage-drop model results which assume the entire applied bias drops linearly across the double-barrier structure.

Clearly, the autonomous oscillations of these RTD simulation results imply the presence of at least two charge storage mechanisms. Following these observations, Buot and Jensen [4] subsequently proposed an equivalent circuit model for the RTD, as depicted in Fig 2a, which incorporated a *constant* quantum-inductance L directly in series with the nonlinear circuit element, I(V). Here, the resulting L |G| product modeled the inherit delay, τ_L, in tunneling across the double-barrier structure through the discrete energy level in the quantum well [14]. Note, this type of time delay, where self-consistent potential effects are ignored, has been recently referred to as the "kinetic" time delay by Landauer [15]. Therefore, in order to produce the characteristics observed in the MBWDF simulations, the RTD equivalent circuit must minimally consist of an inductor-delayed current leg (i.e., quantum-well inductance L in series with a nonlinear tunneling element I(V) of the RTS) in parallel with the double-barrier capacitance. In addition, a series "access" resistance must be included to model the charging delay of the source and drain resistance.

It should also be noted that the "quantum-inductor" model (QIM) of Fig. 2a supports numerical results of Frensley [16] and Kluksdahl, *et al.* [17]. Specifically, their WDF simulations [16,17] had revealed a curious result in the high-frequency response of RTDs subject to small-signal excitation. In particular, an impedance characteristic was obtained with a negative real-part at low frequencies, but with a crossover to positive values at higher frequencies. On the other hand, the traditional "lead-inductor" model (LIM) for an embedded RTD, as given in Fig. 2b, cannot explain this frequency-dependent crossover behavior in the impedance. Note, the LIM circuit-equivalent, which models the intrinsic RTD with a single energy-storage element and attributes any additional frequency-dependence to an extrinsic lead-inductance, is also the one used by the second group (i.e., discussed above) which sought to explain plateau-like I-V behavior by extrinsic effects. Also note that these numerical findings about impedance agree with the QIM circuit with a positive value of inductance; this should be contrasted with another proposed equivalent-circuit model which utilizes a quantum inductance which is negative (i.e., $L = \tau / G$; where τ is the tunneling time and G is the linearized RTD conductance) inside the NDR region [18].

The introduction of a quantum-well inductance, which serves to "choke" the I(V) leg of the QIM circuit in Fig 2a, was able to clarify the important role of electron inertia on the RTDs high-frequency response in the frequency range 10^{13} to 10^{15} Hz. Specifically, when the I(V) leg

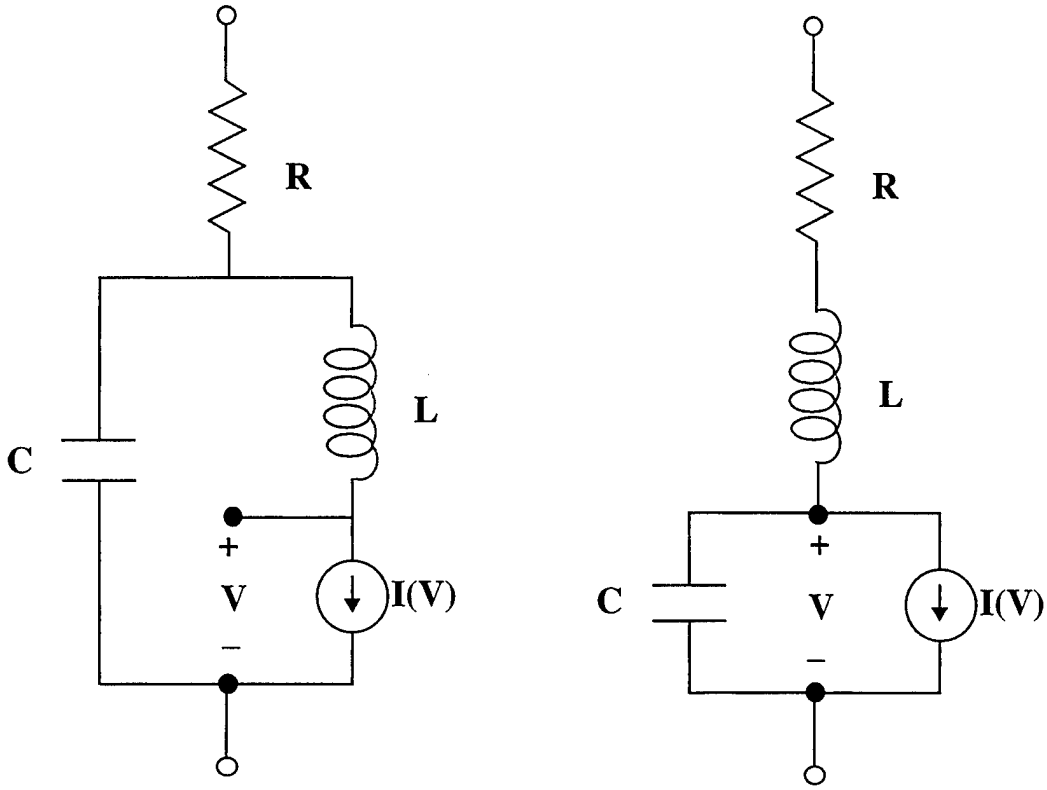

(a) Quantum-Inductor Model

(b) Lead-Inductor Model

FIG. 2. Basic circuit model configurations used in nonlinear oscillation study.

becomes inductively blocked at very high frequencies, the QIM becomes a simple RC circuit which has a purely positive real-part impedance in direct agreement with [16] and [17]. In addition, the QIM's impedance has the ability to become completely inductive in the range 10^{13} to 10^{14} Hz and then to change-back capacitive as the frequency approaches 10^{15} Hz. This dependency of the RTD's imaginary-part impedance also agrees with physics-based simulation results. The QIM circuit is also applicable at frequencies well below the point where inertial effects become significant (i.e., $f \ll 10^{15}$ Hz). At these lower frequencies, the oscillation mechanism can be explained by two characteristic delay times [14]. Namely, τ_B, which is the time necessary to accumulate emitter charge in response to a voltage change and, τ_L, which is the self-consistent averaged time required to "leak" this emitter charge into (and subsequently out of) the well by tunneling. Hence, the condition for formation of oscillations becomes $\tau_B > \tau_L$. This condition applies because if $\tau_B \leq \tau_L$ the emitter charge buildup can rapidly follow in phase with the tunneling process preventing any significant spatial-charge fluctuations between the emitter region and quantum well. However, if $\tau_B > \tau_L$, the accumulated charge in the emitter lags the charge leakage process, leading to a redistribution of charge between emitter and well regions. This time-dependent redistribution of charge is accompanied by a fluctuation of the pertinent energy levels in emitter relative to the discrete RT levels of the well leading to a periodic change in the RTD current. This description of the oscillation process is supported by the numerical simulations in [9] which clearly show an out-of-phase delayed spatial-fluctuation of electron density between the emitter and well regions. Moreover, this fluctuation occurs mainly between a narrow accumulation region in the emitter (i.e., near the first barrier) and the quantum well.

The QIM given in Fig. 2a can immediately be used to deduce relations for the emitter-charging time and the quantum-tunneling delay time. The QIM circuit yields $\tau_B = RC$ and $\tau_L = L/|G|$ where G is the linearized conductance in the NDR region. This circuit configuration can also be used to derive condition-for-oscillation criterion in good agreement with the quantum-based simulation results. Such a "linear" analysis, using the constant-parameter version (i.e., constant R, L and C) of the model in Fig. 2a, has been performed by Buot and Jensen [4]. Applying standard

circuit relations, and transforming the results about the resulting average values of voltage/current for an assumed dc voltage source V_S, yields a dynamical relation for the transient voltage v of

$$RCLG\frac{d^2v}{dt^2} + (RC + LG)\frac{dv}{dt} + R I_L + (RG + 1)v + V_{dc} = V_S \qquad (1)$$

Equation (1) is a linear second-order differential equation which describes the time-dependent component of the total voltage $V = v + V_{dc}$ across the nonlinear current-element I(V) in Fig. 2a. Here, V_{dc} is the dc part of the voltage across I(V) and I_L is the dc part of the current through I(V). Noting the condition that $R I_L + V_{dc} = V_S$, Eq. (1) can be expressed as the "viscous" harmonic oscillator equation

$$\frac{d^2v}{dt^2} + \eta\frac{dv}{dt} + \omega^2 v = 0 \qquad (2)$$

where

$$\eta = \frac{LG + RC}{RCLG} = \frac{1}{\tau_B} - \frac{1}{\tau_L}, \qquad (3)$$

$$\omega^2 = \frac{1 + RG}{RCLG} \qquad (4)$$

and the constant parameter G is the conductance defined in a small neighborhood around the V_{dc} operating point. Specifically, $G = G(V=V_{dc}) = (d\,I/d\,V)\,|_{V=V_{dc}}$ or the slope of I(V) at $V = V_{dc}$. Note therefore, this "linearized" analysis only applies for small displacements about the dc operating point and is useful only for establishing stability criterion relating to the spiraling orbits in phase-space. Depending on the values of the physical parameters, these orbits may spiral outward (i.e., grow) or inward (i.e., decay). Under these linearized conditions, the solution of Eq. (2) is given by

$$v = A\exp(\lambda_1 t) + B\exp(\lambda_2 t) \qquad (5)$$

where

$$\lambda_{1,2} = -\frac{\eta}{2} \pm \sqrt{\frac{\eta^2}{4} - \omega^2} \tag{6}$$

Applying strict conditions for the formation of "limit cycle" oscillations (i.e., negative η and $\omega^2 > 0$) when biased in the NDR region yields [4]

$$\tau_B > \tau_L, \text{ and } R|G| > 1. \tag{7}$$

Hence, a simple linear analysis of the quantum-inductor circuit configuration yields minimal oscillation criterion in direct agreement with the physics-based charge exchange arguments presented earlier. Furthermore, any attempt to explain the MBWDF simulations results using extrinsically-based arguments (i.e., lead-inductance analogy) will fail [19]. This is true because, as shown in Ref. [4], oscillations induced by external lead-inductances will always arrive at exactly the opposite conclusions (i.e., $\tau_B < \tau_L$, $R|G| < 1$). Therefore, this simple analysis has deduced some definite conclusions about the correct circuit-equivalent *configuration* for modeling intrinsic oscillations in RTDs.

Insight into the hysteresis behavior can also be deduced from the self-consistent charge buildup arguments. Indeed, hysteresis in intrinsic RTDs can result as a consequence of charge buildup and ejection from the quantum well. For example, a simple charge transport analysis, using an energy-balance equation and the relaxation-time approximation, can readily show hysteresis behavior [20,21], but without the characteristic plateau-like features. In fact, this type of intrinsic bistability has been demonstrated experimentally [22,23]. In a direct analogy, a circuit loadline analysis of a *constant* access resistance R in series with nonlinear conductance element I(V) will demonstrate hysteresis behavior if $R|G| > 1$. Here, the $R|G| > 1$ condition is necessary to insure multiple loadline intercepts (i.e., since -1/R defines the slope of the loadline and -|G| is the slope of the I(V) function in the NDR region). However, as will be shown in the next section, a constant-R loadline cannot produce the plateau-like region exhibited by quantum simulation results of Fig. 1.

This section has served as a review of previous investigations into the hysteresis and bistable behavior of RTDs. As shown, there is both theoretical and experimental evidence for the existence of intrinsic self-oscillations and bistability in RTDs. While there is a tendency to attribute such phenomenon to extrinsic effects, linear RLC circuit analysis reviewed here confirms the need of including a quantum-inductance effect into the RTD circuit-equivalent model (i.e., as shown in Fig. 2a). Specifically, linear arguments set the inclusion of this quantum-inductance as a necessary condition for producing the intrinsic oscillations and for matching the high-frequency impedance characteristics. Thus, the constant-parameter version (i.e., constant R, L and C) of the circuit configuration given in Fig. 2a has been validated for small-signal excitation when the RTD is biased in the NDR mode.

While these linear-analysis based conclusions provide valuable insight, it is important to note that they cannot fully describe the entire process under investigation. It should be pointed out that the attainment of a limit-cycle phenomenon always arises from the accurate balancing of energy gain (e.g., NDR) and loss (e.g., series resistance) mechanisms which are always nonlinear. For a limit-cycle to establish itself, an equilibrium must be attained where gains and losses are balanced over a complete period. This implies the existence of some parametric dependence (e.g., voltage-dependent conductances) to limit the cycle growth. For example, the previous linear analysis resulting in Eqs. (1) thru (7) will predict oscillations which grow without bound because the NDR conductance is treated as a constant regardless of the value of V. While this type of analysis can give "spiral" start-up criterion, approximate oscillation frequency, and predict the possibility of a limit-cycle by virtue of the nonlinear G, a complete analysis must incorporate all the important nonlinear effects.

Therefore, an analysis which includes all pertinent nonlinear dependencies is required to accurately characterize and understand the intrinsic behavior of RTDs. This is true, not only for discerning features of the self-oscillations, but also for resolving the nature of the overall I-V characteristic. A typical RTD I-V characteristic will possess a hysteresis, plateau behavior, and sharp "jumps" as shown in Fig. 1. As mentioned previously, much of these features are often attributed to extrinsic circuit effects. For example, hysteresis can be produced by a lead-resistance loadline and extrinsic oscillations can introduce shifts in the overall I-V curve. On the other hand, intrinsic charge-storage mechanisms can produce similar results and plateau behavior. However, a unique set of nonlinear

circuit-equivalent mechanisms have not yet been identified which can produce all these features in an *intrinsic* RTD. Hence, the remaining question is concerned with the degree in which the proposed QIM circuit, of Fig. 2a, can reproduce the MBWDF transport results of Fig. 1. Specifically, can this circuit produce a hysteresis and oscillations which combine to yield the overall plateau features. Note, the MBWDF results include discrete "jumps" and a plateau region which increase as a function of forward bias. These are features which could not be resolved using *static* charge-storage arguments (e.g., see [10] or [20]).

In the presentation which follows, the physics of the hysteresis from the equivalent circuit point of view is further considered. Here, fully nonlinear simulations will reveal the *intrinsic* hysteresis to be primarily a dc phenomena that does not necessarily involve the quantum-well inductance or the RTD capacitance. The study will show the correct hysteresis behavior arises when a *nonlinear* resistance R(V) is placed in series with a nonlinear I(V) circuit element. In addition, the introduction of the nonlocal (i.e., depends on the voltage across NDR element) access resistance element is shown to derive oscillatory behavior in direct agreement with self-oscillations obtained from quantum mechanical simulations. Furthermore, nonlinearity effects present in the inductive-delay element are shown to induce a positive-slope plateau region. Hence, the overall hysteresis and bistability phenomenon can be closely tied to nonlinear physical mechanisms present in the intrinsic RTD structure.

III. NONLINEAR EQUIVALENT CIRCUIT MODEL STUDY

To begin, consider the general mathematical relations describing the current/voltage dynamics of the QIM circuit. If the circuit configuration given in Fig. 2a is biased by a dc voltage source V_S, application of standard circuit relations yields the autonomous second-order nonlinear equation

$$\frac{d^2v}{dt^2} + \eta(v, V_{dc})\frac{dv}{dt} + \zeta(v, V_{dc})\left(\frac{dv}{dt}\right)^2 + \omega^2(v, V_{dc})\, v = 0 \qquad (8)$$

where

$$\eta(v, V_{dc}) = (LG(v, V_{dc}) + RC) / (RCLG(v, V_{dc}))$$

$$\zeta(v, V_{dc}) = (G'(v, V_{dc})) / (G(v, V_{dc}))$$

$$\omega^2(v, V_{dc}) = (1 + Rg(v, V_{dc})) / (RCLG(v, V_{dc}))$$

for the transient voltage v across the nonlinear conductance element I(V). Equation (8) has been derived in a current-voltage frame of reference where the total voltage across I(V) is $V(t) = v(t) + V_{dc}$ and V_{dc} is the oscillation-free voltage component. Note, Eq. (8) allows for the possibility of an access resistance R(V) which has a nonlocal dependence on NDR potential. The incorporation of nonlinearity into the circuit model leads to transient (and dc) voltage dependent coefficients

$$g(v, V_{dc}) = (I(v + V_{dc}) - I(V_{dc}))/v \tag{9}$$

which can be defined as the *nonlinear* conductance, since in the defined frame of reference the transient current density is $i = I(v + V_{dc}) - I(V_{dc}) = g(v, V_{dc})\,v$, and

$$G(v, V_{dc}) = G(V) = dI/dV \tag{10}$$

which is just the slope of $I(V)$ at $V = v + V_{dc}$ or the normal definition of the *linearized* conductance. This transformation allows solution of the nonlinear dc biasing separately from the time-dependent oscillation problem. Specifically, the dc bias solution for V_{dc} is obtained from the voltage-drop relation

$$I(V) + \frac{(V - V_S)}{R(V)} = 0 \tag{11}$$

where once again we have allowed for the possibility of a nonlinear access resistance. In order to properly interrogate the nonlinear version of the quantum-inductance model, values (or functions) for the elemental parameters; R(V), L, C and I(V) must be defined. A numerical algorithm must then be implemented to solve both the dc biasing equation in (11) and the dynamical equation in (8) for the unstable (or decaying) transient states. In the two subsections that follow, both of these problems will be addressed by first considering the oscillation-free characteristics and then progressing on to the oscillation modes corresponding to the RTD structure studied in Ref. [4].

A. Oscillation-Free Characteristics

This section will consider the stable (oscillation-free) current solutions which result from the quantum-inductor RTD circuit configuration of Fig. 2a. For this dc analysis (and for the oscillation

study of the next section) an RTD structure will be considered which was previously studied using a Wigner-distribution-based physical model. Specifically, a GaAs-$Al_{0.3}Ga_{0.7}As$ double barrier structure with 30 Å barriers and a 50 Å well. The entire device, including 2.0×10^{18} cm^{-3} doped equal-length source and drain buffer-regions, is 550 Å in length. A temperature of 77K is assumed throughout. The potential barrier heights used are 0.3 eV and an electron effective mass of $0.0667m_0$ is assumed throughout the device structure. To derive the dc characteristic, Eq. (11) must be solved which contains the nonlinear conductance I(V) and access resistance R(V).

To begin, the traditional approach of assuming a constant-R will be investigated. The results given in Fig. 1 can be used to derive both the constant-R value and the I(V) conductance function. As shown, Fig. 1 gives the overall self-consistent current-density results for the structure under consideration. Since this self-consistent result includes the influence of the buffer regions, it inherently contains information for determining the access resistance. Figure 1 also contains the linear voltage-drop results which were obtained by applying the entire potential-drop linearly across the barrier-well-barrier structure. Note, the linear voltage-drop results correspond to a zero value of R; hence, this result provides a description for the intrinsic device conductance I(V). Since a constant access resistance would lead to a uniform shift in the overall I-V curve, the constant R value can be estimated from the resulting shift of the peak-current-point in Fig. 1 when self-consistency is included (i.e., by comparing the linear voltage-drop result to self-consistent result [4]). Employing this approach yields $R = 1.63 \times 10^{-7} \Omega\ cm^2$.

At this point, a set of constant-R loadline intercepts for the quantum-inductor circuit can be obtained by solving the nonlinear voltage-drop relation in Eq. (11). In this case Eq. (11) defines the intersections of the nonlinear conductance I(V) and the linear relation $(V - V_S) / R = 0$ which uniquely defines the stable current solutions. Figure 3 illustrates a discrete set of these intersection curves for three values of applied bias. From continuity considerations, the overall oscillation-free I-V curves may be plotted as shown in Fig. 4. Figure 4 contains solutions for the forward and backward bias sweeps as well as for the tri-stable (i.e., middle current solution) states. Note, the hysteresis results of Fig. 4 closely resemble those obtained from a simplified analysis of charge-storage effects in RTDs given by Sheard and Toombs [20].

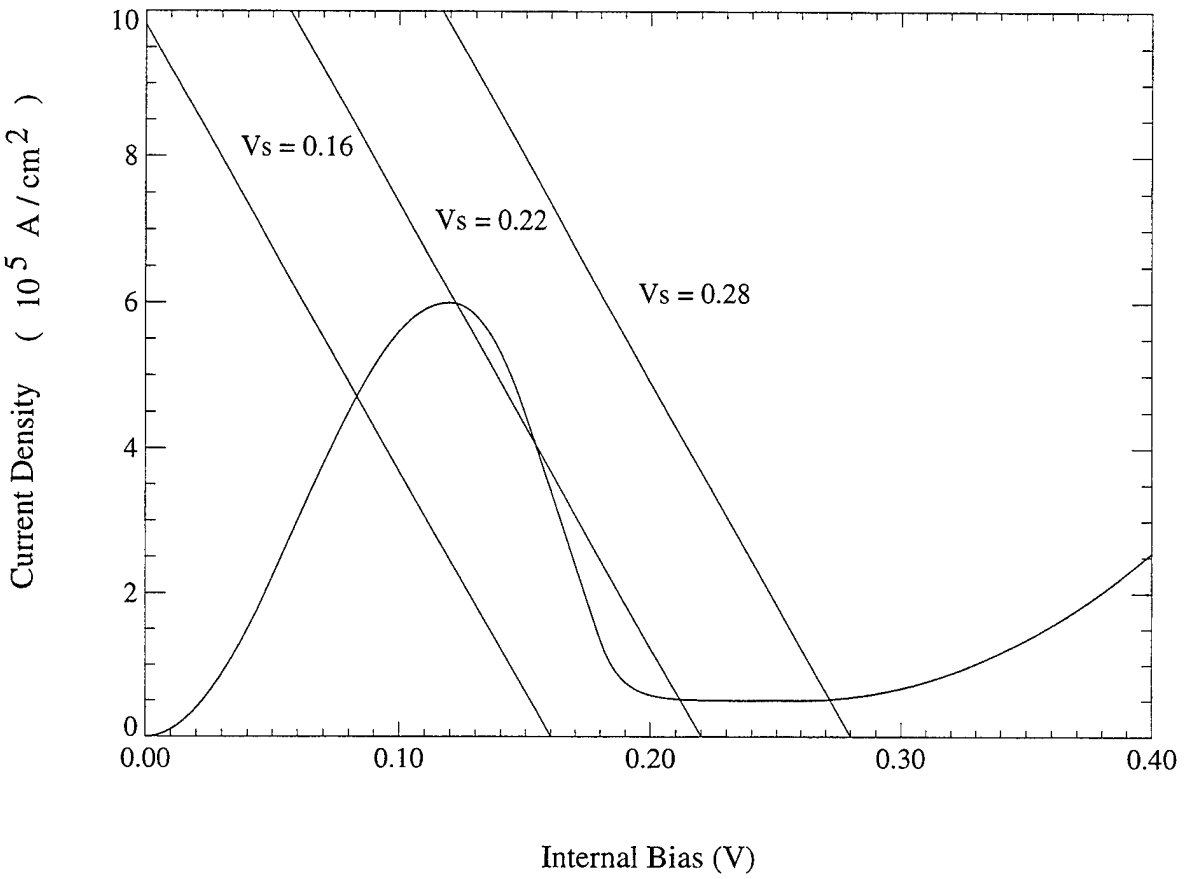

FIG. 3. Intersection curves of *I(V)* characteristic and loadline for three different applied biases.

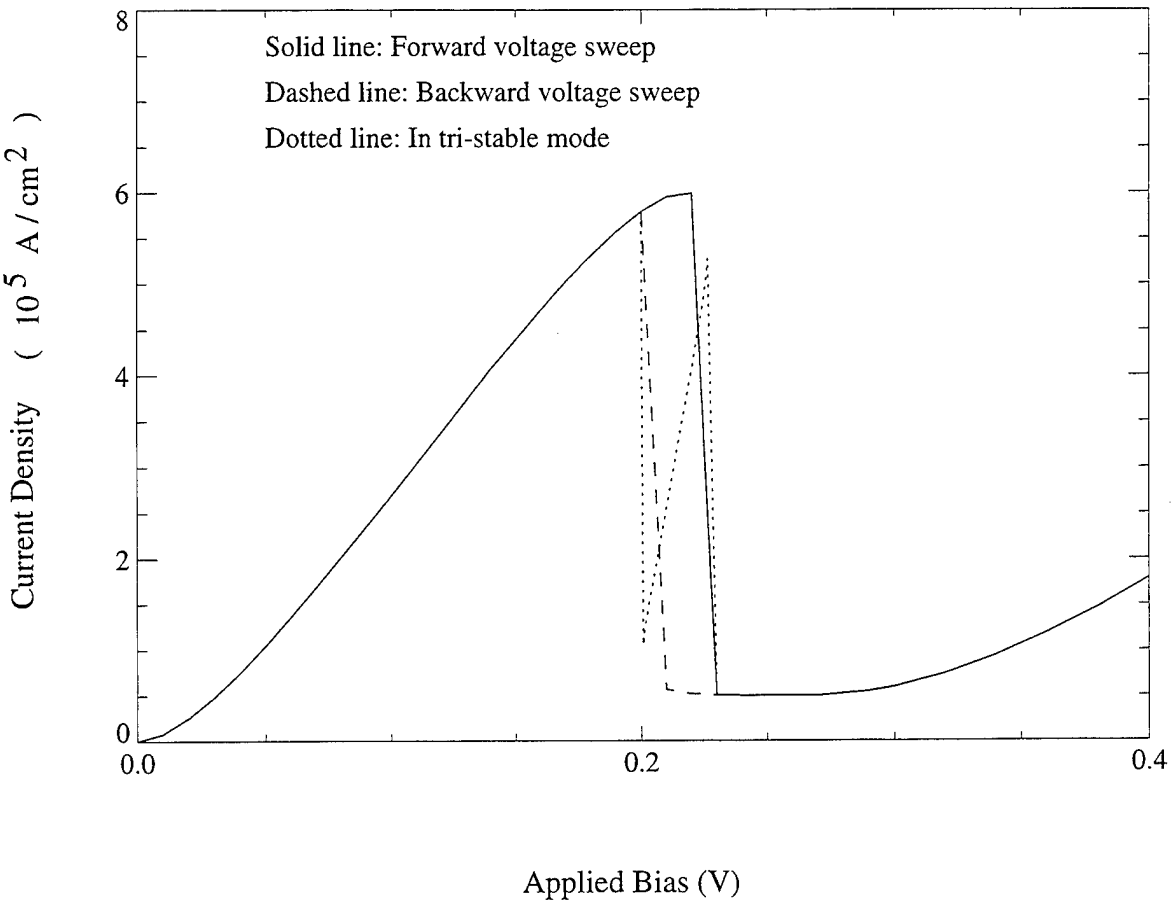

FIG. 4. Overall current-density load-line solutions for forward, backward, and tristable states. Note, this excludes any oscillation effects.

The constant-R results of Fig. 4 lack the plateau-like structure distinctly present in the quantum simulation results of Fig. 1. It is well known that multiple energy-storage circuits possess the potential to produce autonomous oscillations and that the presence of such oscillations can lead to displacements in the overall I-V curve [24]. Thus, one might incorrectly attribute the entire absence of step-like behavior (i.e., in Fig. 4) to the exclusion of transient effects by this dc analysis. Clearly, if oscillations with limit-cycles (i.e., non-decaying modes with identically repeating cycles) were to result when biased in the NDR region, one could correctly anticipate some change to the time-averaged I-V characteristic. This is true because the conductance relation I(V) is nonlinear; therefore, the forward and backward swings in current will be different.

To explore this issue in detail, a comprehensive study has been performed to derive the nonlinear oscillations of both the quantum-inductor and lead-inductor models given in Fig. 2. This comprehensive study utilized numerically generated results to extensively evaluate the two circuit configurations for various nonlinear effects [25]. In the next section, details useful in explaining the intrinsic oscillation process in RTDs will be presented. However, at this point it is important to note that the constant parameter models (i.e., constant R, L and C) were unable to match the physics-based results of Ref. [4]. In particular, while I-V curves with qualitative features similar in some respects to those observed both theoretically and experimentally (e.g., see Ref. [3]) were obtained, there were some major differences. For example, Fig. 5 shows the overall I-V results obtained for the constant-R quantum-inductor model (note, values of $L = 1.48 \times 10^{-21}$ H cm^2 and $C = 2.3 \times 10^{-7}$ F / cm^2 were estimated from oscillation-mode data). As shown, differences included an excessively large value of current in the plateau region and a very narrow hysteresis region. A variational study of the circuit parameters (i.e., L, R and C) was also performed which revealed no marked improvement could be obtained using the constant parameter model. Thus, it is obvious that a constant R, L and C model cannot be used to represent all the nonlinear dynamics over the entire NDR region [15].

Up to this point, the analysis has assumed that the bulk access regions are ohmic with a constant resistance representation. Of course, this assumption is true only in the cases where the current is a linear function of the access-region voltage-drop. This is generally true if the applied voltage creates a constant electric field throughout the region where the voltage drop is applied and there

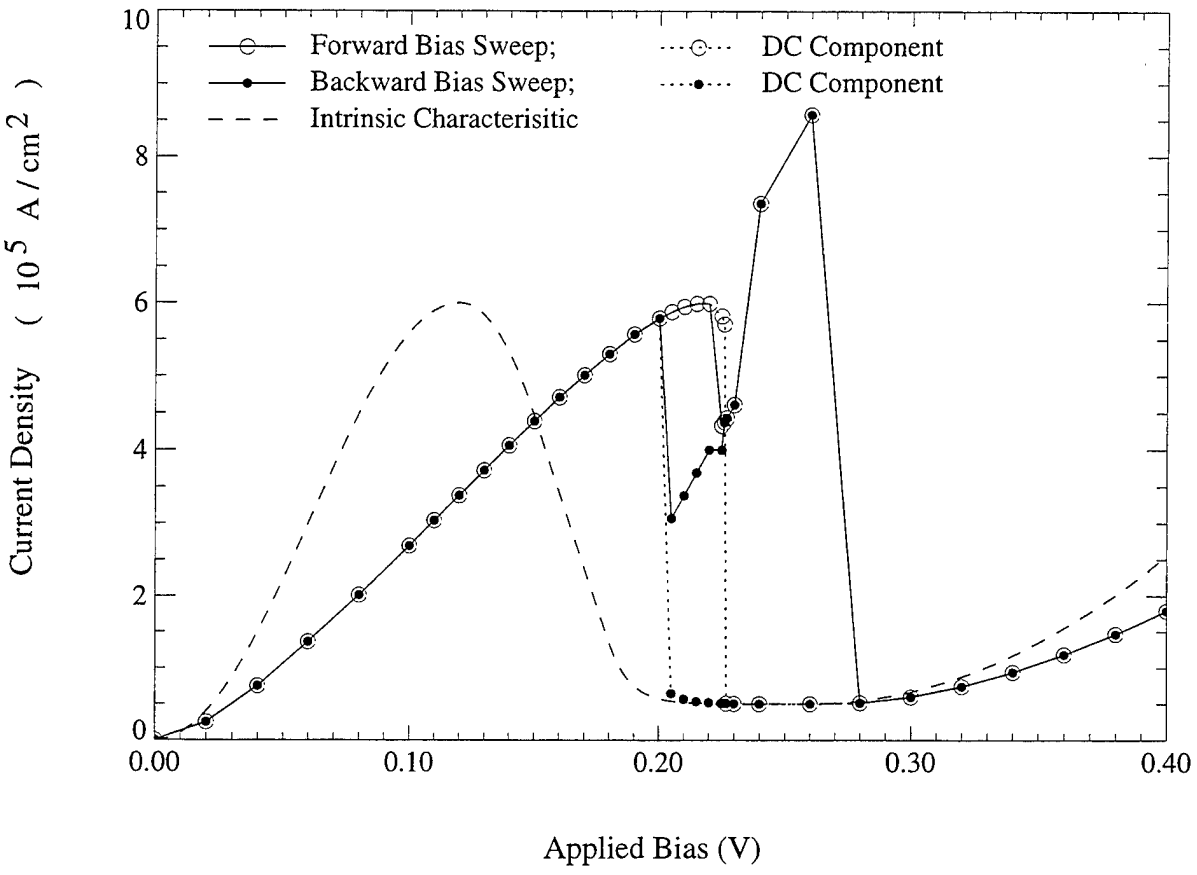

FIG. 5. Overall current density *vs* applied bias derived from quantum-inductance circuit model with constant parameters.

is no accumulated/depleted spatial charge, as in metals. However, in the source region of an RTD where part of the access resistance is defined (similar arguments hold for the depletion charge in the drain region although this region is not as critical to the argument), stored electron charge resides principally in a narrow accumulation region adjacent to the first barrier. This stored charge renders the access resistance to be highly nonlinear and is therefore expected to exhibit a maximum as a function of bias. This is indeed shown by the Wigner-distribution-function simulations of the RTD at 300K [13] and at 77K [19].

The I-V curves obtained from the numerical solution of the quantum transport equation (i.e., Fig. 12c of Ref. [7] and Fig. 2 of Ref. [3]) were used to deduce the nonlinearity of the access resistance R(V) as a function of applied bias. Figure 6 shows a simple piece-wise approximation to R(V) obtained from a point-by-point estimation of the shift between the two current-density functions given in Fig. 1. Since the dc R(V) is sought (i.e., need access resistance which exists in the absence of the intrinsic oscillations), the function displayed in Fig. 6 was derived using the backward leg of the self-consistent I-V curve which is essentially free of oscillations.

The explanation for why R(V) was obtained from the backward leg of the hysteresis data is really quite simple. Here, equivalent-circuit element values are being derived from the quantum simulations in much the same way an experimentalist might extract these values from a real device. Since the real device is really a black box, a circuit equivalent is assumed and then a match to the parameters is extracted from the measurement data. However, when self-oscillations exist they can shift the overall time-averaged I-V results. Hence, if the goal is to completely match to this time-dependent data one needs to solve for the oscillation behavior. In fact, such time-dependent studies will be presented later in the self-oscillation subsection. However, at this point some method is needed to identify the dc voltage dependence of the access resistance. Now, since the backward-leg hysteresis data of the quantum simulations is mostly stable (i.e., with only a very narrow unstable bias-region), it can be used to obtain the dc R(V) characteristic. Hence, this purely dc R(V) function is free of any time-dependent influences (i.e., shifts due to self-oscillations) and can be used as a model parameter for both forward and backward sweep calculations.

Also note the access resistance model is defined as a nonlocal function of voltage across the nonlinear conductance element I(V). This parameterization is truly a nonlocal feedback effect

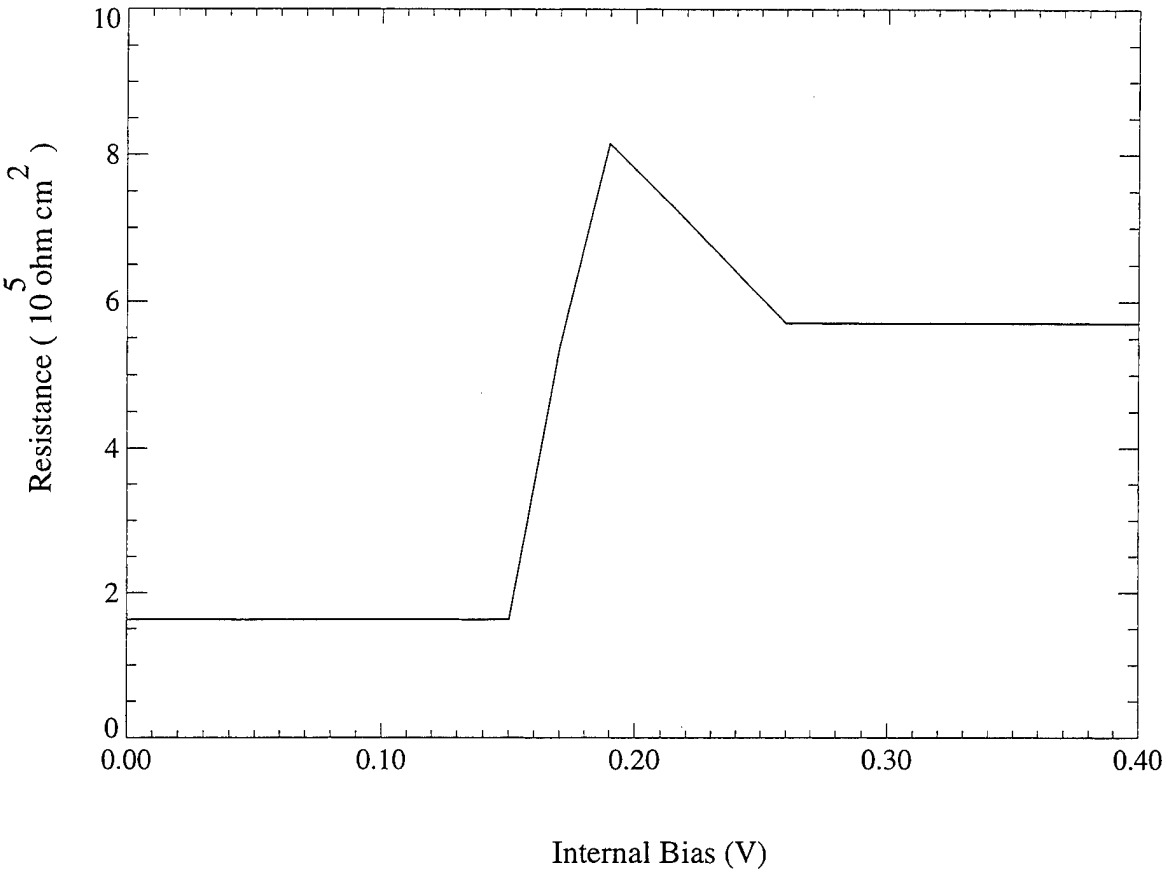

FIG. 6. Access resistance *R(V)* as a function of voltage across the intrinsic RTD structure.

since a unique mapping to the bulk-region potential does not exist under transient conditions (i.e., when the R(V) and I(V) elements of Fig. 2a are electrically separated by the inductor element L).

The R(V) result in Fig. 6 exhibits a step-like characteristic at a bias corresponding to the onset of NDR region. When this nonlinear resistance model is incorporated into the quantum-inductor circuit configuration, the results for the dc circuit (i.e., R(V) in series with I(V)) are drastically altered. Figure 7 gives a new set of loadline intercepts and shows how the nonlinear R(V) introduces sag into the characteristic as compared to the linear R loadline shown previously in Fig. 3. The resulting dc component of the I-V characteristic, given by the dashed-line results in Fig. 8, already contains the desired step-like behavior observed in the physical-model results of Fig. 1. As can be seen by comparing Figs. 3 and 4 to Figs. 7 and 8, the sag in the nonlinear loadline extends the voltage-range over which the hysteresis persists. This improves the agreement between the equivalent circuit results and the physics-based simulations. Also note, this dc hysteresis agrees with previous experimental observations of intrinsic RTD behavior [10].

This dc hysteresis effect is a very interesting result since it shows that, aside from limit-cycle oscillations in the NDR region, a nonlinear access resistance contributes to the plateau-like behavior of the overall I-V characteristic. In fact, as the next section will show, R(V) is the major cause of the hysteresis behavior and an important factor in determining the self-oscillation phenomenon in this RTD structure.

It is important to note that this dc bistability effect obtained for this particular intrinsic device structure will not apply globally to all RTDs. This is true because the overall character of this intrinsic hysteresis phenomenon arises from charge accumulation both in the well and emitter region. It is well known that the total accumulation of charge will depend on device area and on the degree of asymmetry of the double barrier structure [22]. Furthermore, subtle changes to buffer layer doping near the barrier interfaces may strongly influence the results. In fact, previous experimental verification of intrinsic dc bistability in RTDs has required the use of highly reflective collector barriers to enhance electrostatic feedback [22,23]. It is true that many experimental observations of bistability are due to *extrinsic* circuit oscillations and/or the coupling of a large external series resistance in series with the NDR of the diode. However, it is also true that either of these effects could prevent the observation of a truly intrinsic bistability [23].

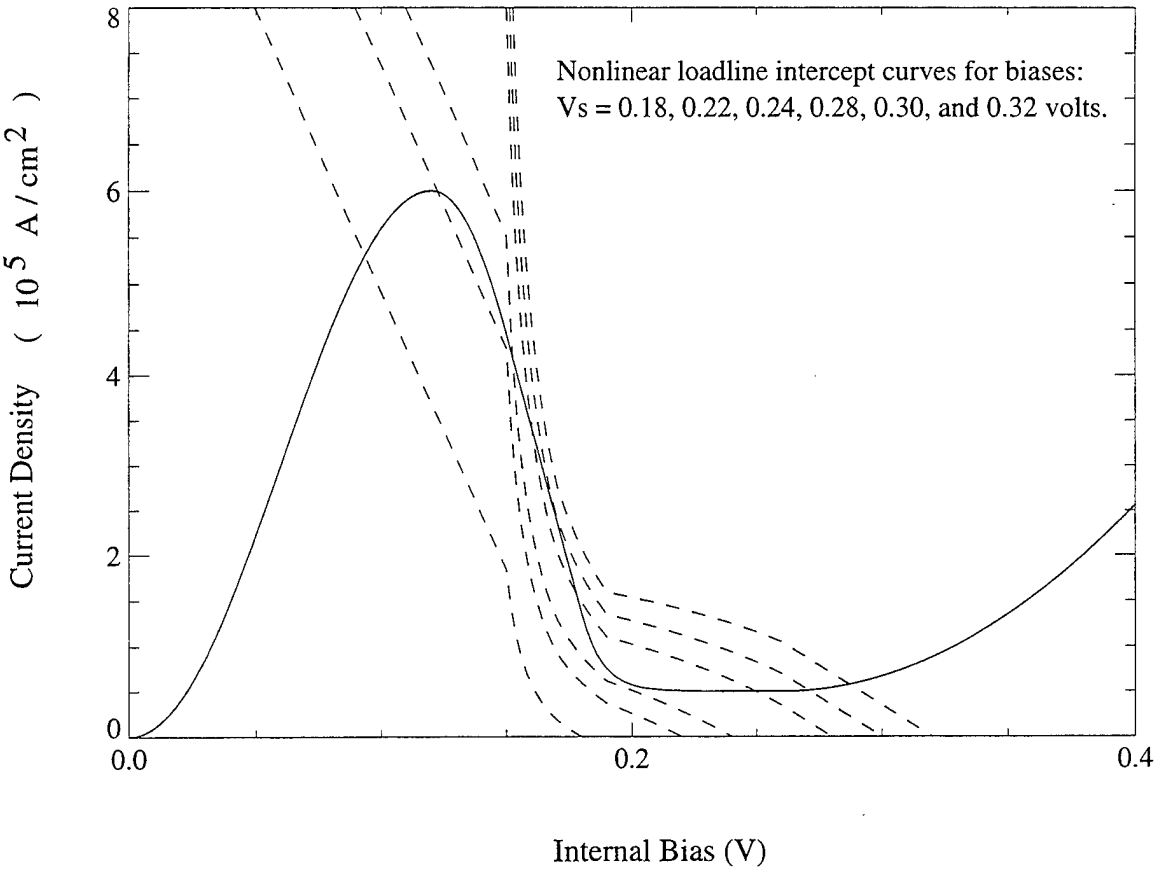

FIG. 7. Nonlinear *R(V)* load-line intersection curves for a number of applied biases.

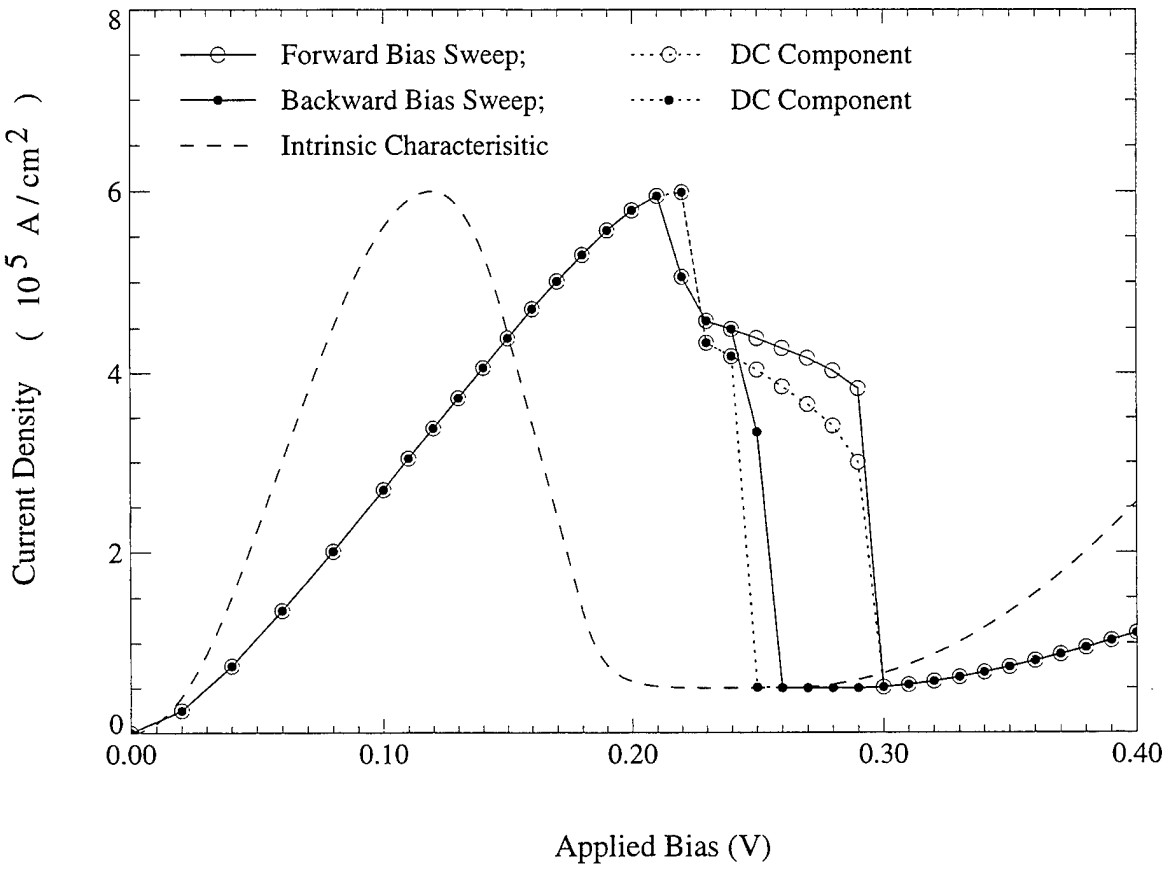

FIG. 8. Overall current density *vs* applied bias derived from quantum-inductance circuit model with nonlinear *R(V)* model.

Therefore, since this intrinsic dc bistabilty is dependent on device area and symmetry, its existence is not necessarily contradicted by experimental results which show that some RTD structures can often be biased in a stable fashion (i.e., so they do not exhibit a hysteresis) either by reducing the device area or by reversing the sign of the applied bias. This work is concerned with developing an equivalent circuit model essentially for an intrinsic RTD (i.e., bulk access regions are less than 250 A) and that the nonlinear resistance arises from a very short charge-accumulated region adjacent to the barrier structure. In realistic device structures, additional contact resistance will also be incorporated in the R(V) characteristic and this constant component will strongly influence the voltage shift and extent of the hysteresis. Since it is well known that reducing the area of a whisker-contacted device will reduce the skin-effect component of the contact resistance [26], a particularly large-area RTD structure which might exhibit intrinsic bistability may not show this effect when the area is reduced. This also agrees with the $RC > L|G|$ criterion for oscillating behavior since for these cases R and C are reduced, resulting in the absence of plateau-like behavior. Note that for the values of the nonlinear R(V) used in deriving the loadlines of Fig. 7, the criteria for oscillatory behavior in the NDR (i.e., $RC > L|G|$ and $R|G| > 1$) are still satisfied.

B. Self-Oscillation Study

To investigate the effect of self-oscillations, a numerical simulation study of both the QIM and LIM circuits was performed [25]. In these investigations, the circuit models were interrogated for their ability to match the quantum-simulation results of Ref. [4]. Specifically, an agreement to the overall I-V curves in Fig. 1 and an approximate amplitude/frequency match to the quasi-harmonic self-oscillations (i.e., see Figs. 2 and 3 in Ref. [4]) is desired. Studies were performed which utilized both a constant access resistance (i.e., $R = 1.63 \times 10^{-7} \Omega\ cm^2$) and the nonlinear functional R(V) as defined in Fig. 6. In these studies, linear arguments (e.g., oscillation frequency) were employed to estimate *initial* values for the energy-storage elements of $L = 1.48 \times 10^{-21}\ H\ cm^2$ and $C = 2.3 \times 10^{-7}\ F/cm^2$. Since all possible voltage-dependencies present in these energy-storage elements could not be directly extracted from the results of Ref. [4], variational studies over ranges of L and C were also performed for

completeness. For the cases involving the QIM circuit, nonlinear inductance effects were considered by performing calculations using a quantum-well inductor which depends on NDR conductance. Here two different but related models were investigated. The first investigations utilized a *positive* inductor model defined by $L = \tau/|G(V)|$ where τ is the quasibound state lifetime. A subsequent study employed a *negative* version (i.e., within the NDR region) of this model where $L = \tau/G(V)$. Note, this negative-L model was previously derived by Brown *et al.* [18] using a linearized impedance analysis.

In this work, a van der Pol algorithm [27] was employed to solve Eq. (8) (and various other versions for the nonlinear-L QIM circuit studies and LIM circuit studies) for the nonlinear phase-space trajectories and the final current-density limit cycles were averaged to arrive at the overall I-V characteristics. While the circuit configuration of Fig 2a appears rather simple, it should be noted that the inclusion of nonlinear elements can lead to *jumps* at the turning points of the phase-space trajectories [25]. These allowable jumps in the current-density (e.g., see Fig. 10) correspond to instances where dv/dt is discontinuous which is a phenomena that can be explained on physical grounds. Specifically, current jumps result when conditions conspire to allow the phase-space (i.e., $z = dv/dt$ verses V) trajectory to intersect the boundary of the NDR region. At the NDR boundary, where $G \rightarrow 0$, consistency in Eq. (8) demands $dv/dt \rightarrow \infty$; however, since Eq. (8) degenerates to a first-order equation a unique solution for dv/dt can be defined [25]. This jump condition, which appeared only in simulations of the QIM circuit, requires special treatment during the iteration steps of the numerical algorithm. Hence, this factor makes the circuit with a quantum inductance much more difficult to solve in comparison to the model with a lead-inductance.

As noted in the previous section, neither equivalent circuit model could reproduce the physics-based results of Ref. [4] when constant parameters (i.e., R, L and C) were employed. For example, Fig. 5 shows the overall (i.e., time-averaged) I-V results obtained from the QIM circuit. Here, the dc current-density component and the intrinsic I(V) characteristic are included for reference. As shown, the oscillatory behavior introduces a large upward-shift yielding a peak in the I-V much larger than that in Fig. 1. In addition, oscillatory behavior was observed to shift the results inside the loadline-induced hysteresis voltage range (0.20, 0.23). Figure 9 plots the current-density phase-space trajectories, corresponding to both the forward and backward bias sweeps, at an applied bias

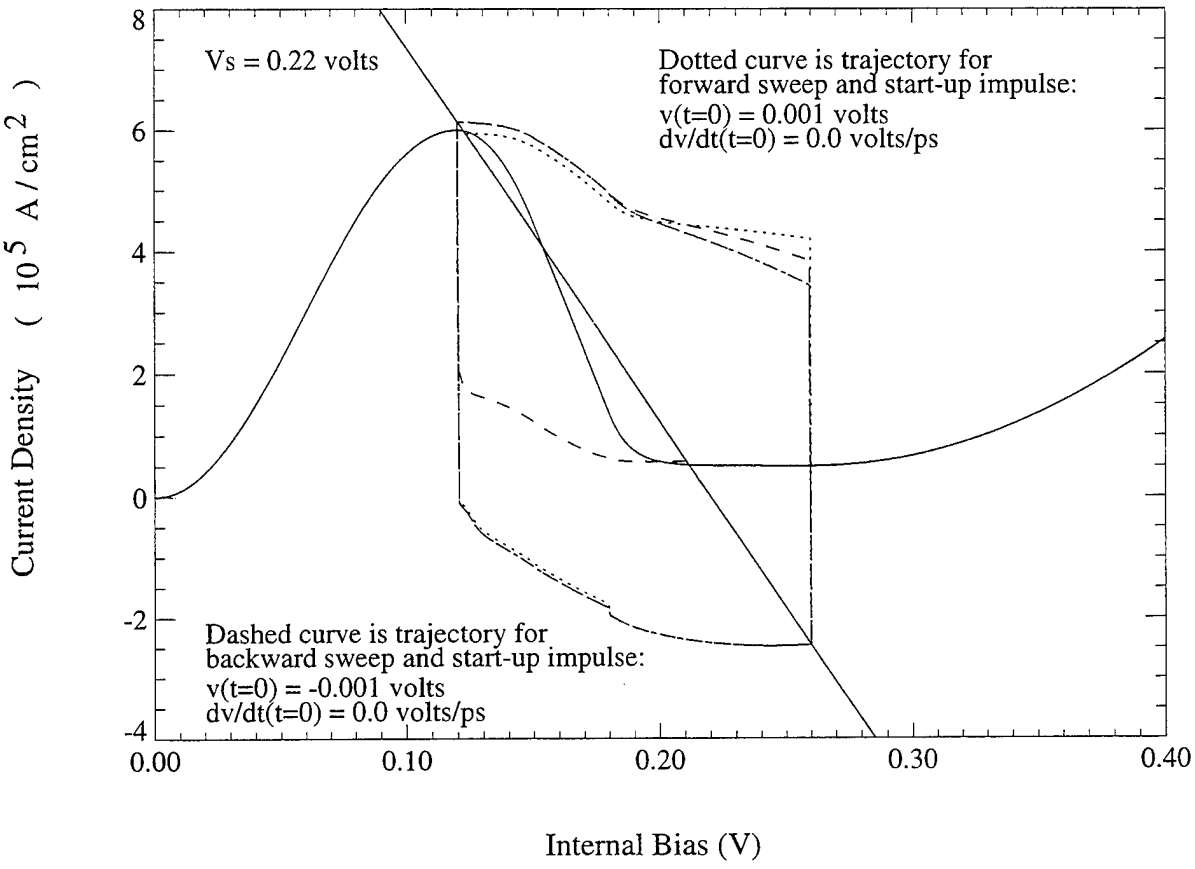

FIG. 9. Current-density phase-space trajectories obtained from constant-R quantum-inductor model for forward and backward bias sweeps at an applied bias of 0.22 V.

of 0.22 volts. For this case, the forward and backward limit-cycles are identical; however, they have opposite-directed shifts which yield approximately the same overall value of current-density. The limit-cycles of Fig. 9 exhibit rapid (but finite) changes in current-density that result from actual z-V phase-space jumps. This point can be made clear by considering the time-domain representation of the forward-sweep trajectory given in Fig. 10. As shown, these jumps in current-density correspond to instances where $z = dv/dt = 0$. Additional variational studies revealed that the constant-R QIM circuit was not able to reproduce the physics-based results. Specifically, this model could not yield the correct plateau-structure or simultaneously match the amplitude and frequency of the quasi-sinusoidal self-oscillations generated by the quantum simulations. Similarly, the constant-R LIM circuit was found to be inadequate [25]. Here, a simultaneous match to overall I-V and oscillation behavior could not be achieved.

A comprehensive study of the LIM circuit, which included the nonlinear R(V) element, verified that it was unable to match either the overall I-V characteristics or the time-dependent behavior obtained from the physics-based results. Conversely, a study of the QIM circuit configuration with the nonlinear R(V) element yielded overall current-density results in very good agreement with the quantum transport simulations of Fig. 1. Figure 8 displays the overall I-V results, for forward and backward sweeps, obtained using the base circuit parameters $L = 1.48 \times 10^{-21}$ H cm^2 and $C = 2.3 \times 10^{-7}$ F / cm^2. Specifically, a forward sweep plateau of approximately the correct magnitude (i.e., $\approx 4.5 \times 10^5$ A / cm^2) and extent (i.e., V = 0.23 to 0.30 volts) is present. In addition self-oscillations were present within the forward-sweep plateau region in direct agreement with the physical simulations. Furthermore, when the base inductor value was tuned to $L = 5.5 \times 10^{-21}$ H cm^2 a very good frequency-match was achieved over the entire plateau-region without any significant influence to the overall I-V plot in Fig. 8. For example, Fig. 11 gives the time evolution of the current-density at two applied bias values in the plateau region. As shown, the periods are 0.3 ps and 0.17 ps at $V_S = 0.26$ volts and 0.28 volts compared to results in Ref. [4] of 0.4 ps and 0.133 ps, respectively. While an exact match to oscillation amplitude was not achieved, the QIM circuit was shown to possess all the basic features present in the physics-based results.

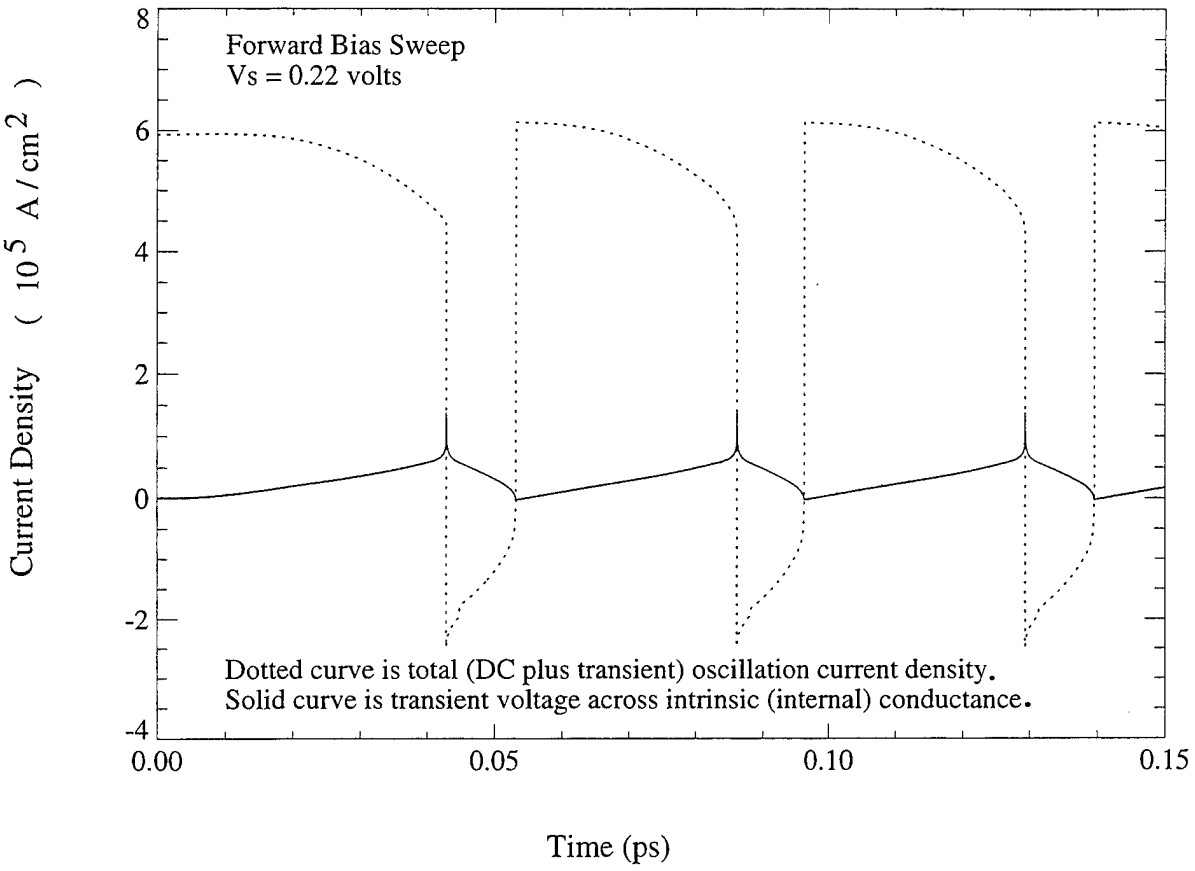

FIG. 10. Time evolution of the total current density for the forward bias sweep of Fig. 9. Here, the internal conductance bias (scaled by a factor of 10 in volts) is also plotted for reference.

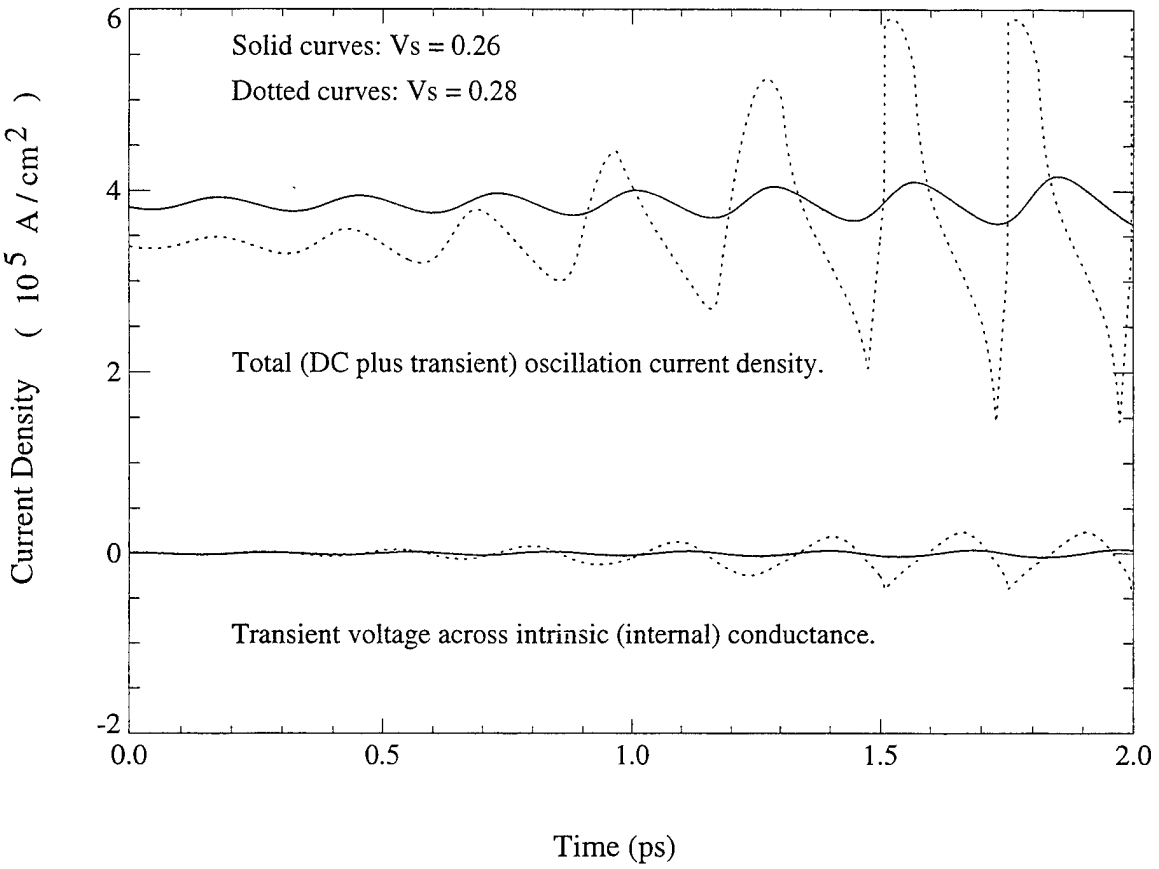

FIG. 11. Time evolution of the total current density, in the quantum-inductor circuit model with nonlinear *R(V)* model, for the forward bias sweep at applied biases of 0.26 and 0.28 V with L = 5.5 x 10^{-21} H cm^2. Here the internal conductance biases (scaled by a factor of 10 in volts) are also plotted for reference. Note, upper curves are current densities and lower curves are internal biases.

It is interesting that the major influence of the nonlinear R(V) can be seen in the dc component of the I-V characteristic alone. The presence of this dc hysteresis effect agrees with previous experimental observations [10] which attributed such intrinsic bistability to interactions between quantized emitter states and RT well states. In addition, the results in Fig. 8 show that the main influence of the self-oscillations is to contribute a slight upward shift to the forward-sweep current density. The inability of the model to amplitude-match the oscillation behavior and the absence of a positive slope in the plateau region suggest improvements to the QIM circuit are needed. The time-dependent characteristics of any dynamical system are strongly influenced by the charge-storage elements. Since estimates of device capacitance, for the RTD structure under consideration, showed a weak bias dependency within the NDR region[4] the nonlinear effects of L will be considered in this work. As discussed earlier, the introduction of L into the equivalent circuit was to model delay effects associated with tunneling. This tunneling delay [14] can be related to the circuit parameters by $\tau_L = L/|G|$. From physical considerations, τ_L should be weakly dependent on applied bias. Therefore, the quantum inductance may be approximated by

$$L = \frac{\tau_L}{|G(V)|} \tag{12}$$

with a nonlinear voltage-dependence that is derived from the NDR conductance. Note, the previous expression for L(V), which predicts positive inductance values within the NDR region, is opposite in sign to the one derived independently by Brown *et al.* [18] where $L = \tau_L / G$. The intrinsic dependency of $G(V)$ can be determined from the linear voltage-drop I(V) curve given in Fig. 1. For the RTD structure under consideration, we estimate the value of τ_L to be 0.06 ps [14] which is in approximate agreement with the independent tunneling calculations of Bahder, *et al.* [28].

Repeating the numerical circuit simulations with the L(V) defined in Eq. (12) yielded the forward-sweep I-V characteristic shown in Fig. 12. Comparing these results to those for a constant L given in Fig. 11 reveals the development of a completely new feature. Specifically, a horn (i.e., with positive slope) is seen to develop within the plateau region which increases with increasing bias until the hysteresis is quenched. This is a characteristic observed in the physics-based results given in Fig. 1. This upward shift in average current density can be understood by comparing the

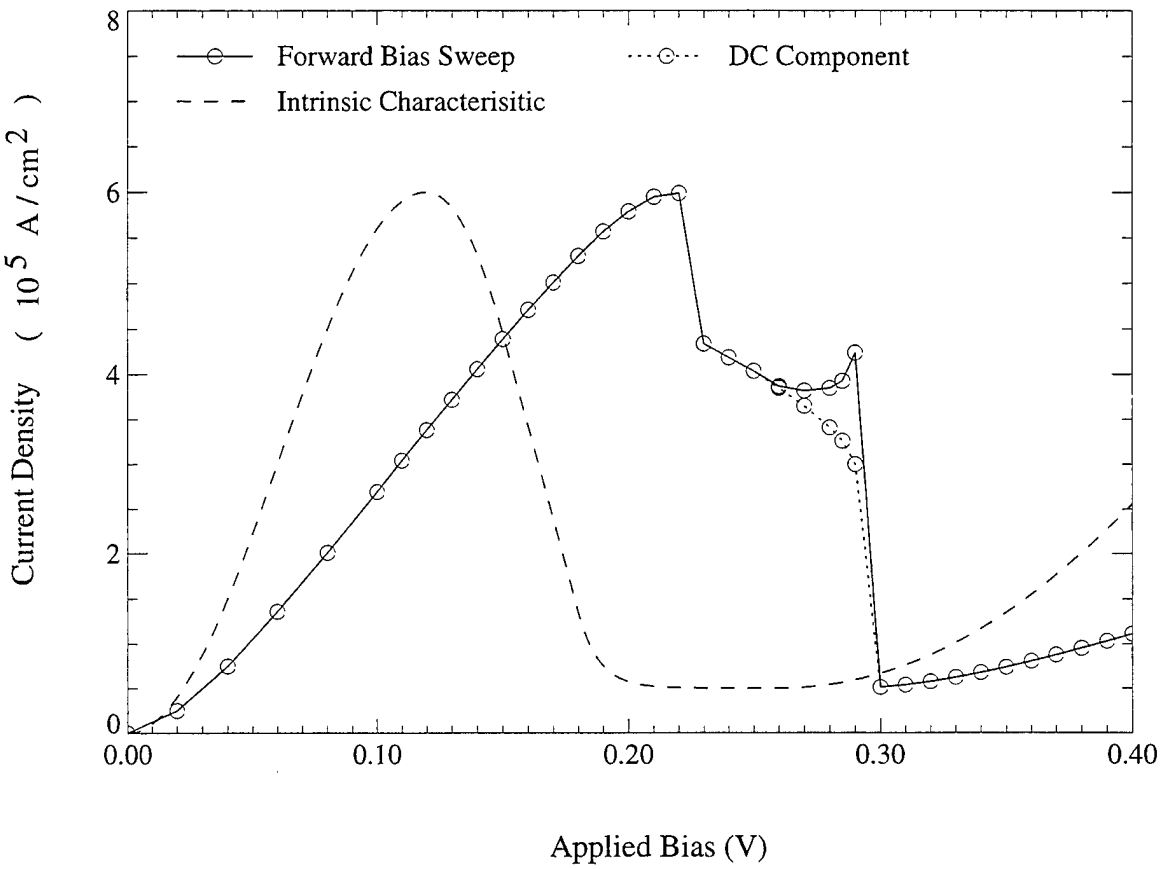

FIG. 12. Overall current density *vs* applied bias derived from quantum-inductor circuit configuration with nonlinear *R(V)* and *L(V)* models.

V_S = 0.28 volt limit-cycle of Fig. 13 to the V_S = 0.29 volt limit-cycle of Fig. 14. For each trajectory, the part of the cycle corresponding to positive values of transient voltage v (i.e., $V > V_{dc}$) is restricted more than for negative values. This is true because the nonlinear inductance is inversely proportional to $G(v, V_{dc})$. Hence, for the positive v part of the cycle the trajectories are impinging upon the flat part of the intrinsic I(V) characteristic where the inductance becomes large. Thus, as the bias is increased the positive part of the v swing is inhibited more by this large inductive effect. In turn, this reduces the negative part of the transient current density in relation to positive component. Therefore, there is a upward shift in the overall current density for this range of biases.

Unfortunately, unrealistically large oscillations were encountered during the backward voltage sweep within the NDR. One possible explanation is a weak nonlinearity associated with the RTD capacitance inside the NDR region. Evidence for such a nonlinear capacitive effect is present in the work of Ref. [1] which suggested different C(V)'s for the forward and backward voltage sweeps. For reference, application of Brown's *negative*-inductor model lead to plateau features and NDR region oscillations which could not be matched (i.e., by variational studies) to the physics-based results [25].

Finally, note that the amplitude of the oscillations is expected to be roughly proportional to the difference of the kinetic delay time, τ_L, and the charge build-up time, τ_B, or $\mathcal{A} = \mathcal{H}\{\tau_B - \tau_L\}$ $\Theta(\tau_B - \tau_L)$ where $\mathcal{A}$ is the oscillation amplitude, $\mathcal{H}$ is the proportionality constant, and $\Theta(\tau_B - \tau_L)$ is the step function. Hence, the L and C elements play a significant role in overall dynamical behavior. Since we cannot directly extract the form of the nonlinearity for L(V) or C(V) from the simulation results in Ref. [1], we suspect this is the origin of the unconstrained oscillations in the backward sweep. Currently, additional work is underway to derive analytical expressions which will offer better approximations to the nonlinear inductive and capacitive effects of the RTD.

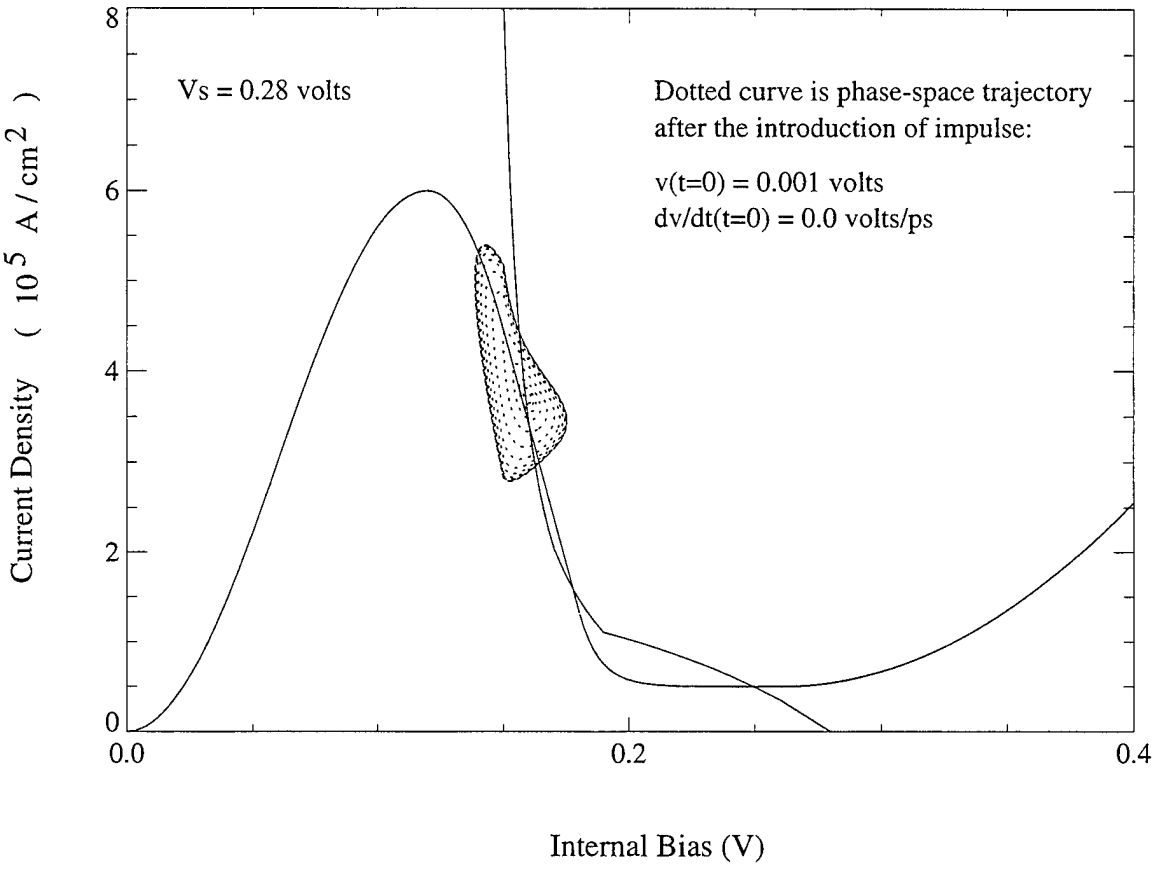

FIG. 13. Forward-sweep current-density phase-space trajectory for $V_S = 0.28$ V.

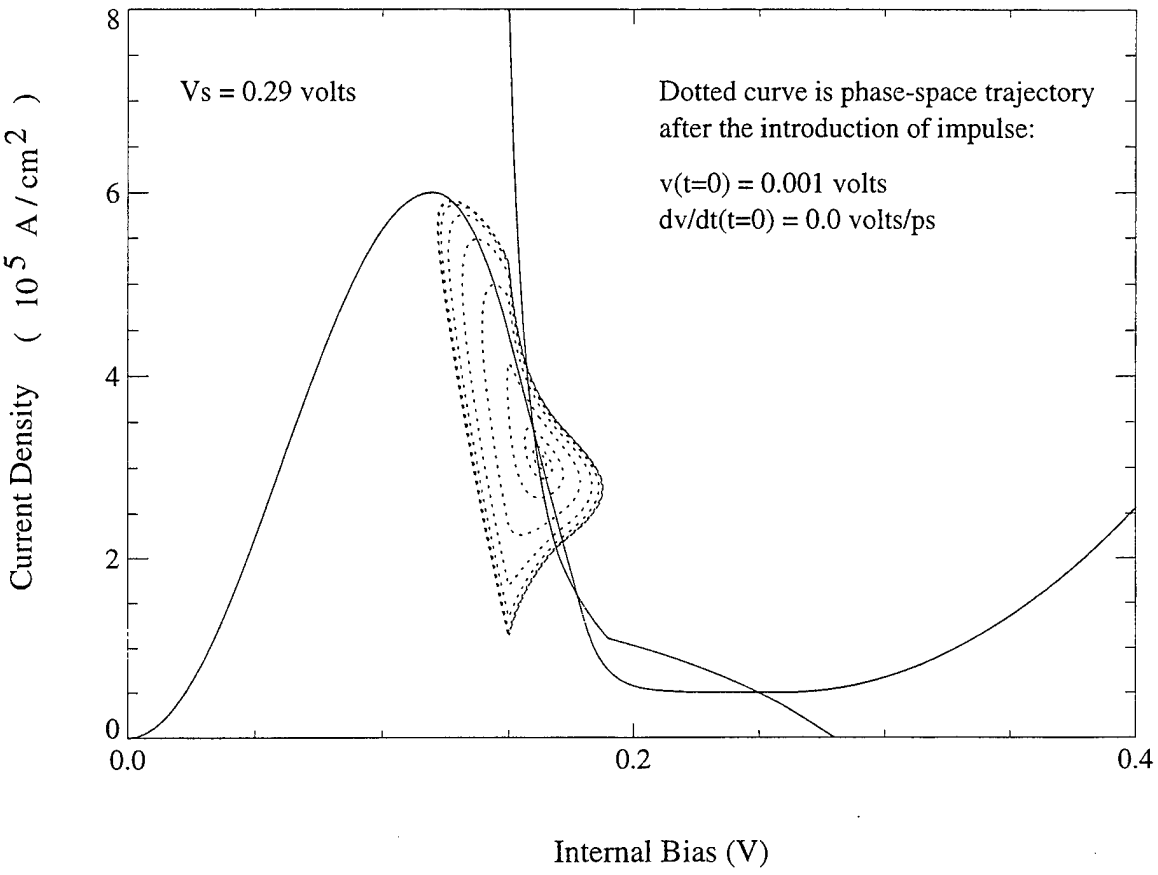

FIG. 14. Forward-sweep current-density phase-space trajectory for $V_S = 0.29$ V.

IV. CONCLUSIONS

These studies have investigated the physics of hysteresis behavior and the physics of limit cycle oscillations in RTDs. This work has combined nonlinear circuit solutions for the limit-cycle oscillation problem with quantum-mechanical simulation results to deduce an improved circuit description for the RTD. Here, the nonlinear coupling between a charge-accumulated access region and the quantum well was shown to produce the plateau-like hysteresis behavior observed both theoretically and experimentally. In addition, the RTD self-oscillations were shown to be intrinsically tied to a quantum-inductance delay effect and, together with the hysteresis, also depend on the nonlinear conductance in the NDR region. This work has shed light on the physical dynamics intrinsic to tunneling structures under bias and offers an improved tool for the optimization of RTDs embedded inside a biasing circuit. Most important, this work provides a nonlinear equivalent-circuit approach for describing the oscillatory dynamics of RTDs and characterizes the dependencies present in the charge-storage mechanisms within the intrinsic device structure. These observations are very important because intrinsic-based oscillations, which do not require the introduction of external resonating elements through contacting resistances, have the potential of achieving operating frequencies in the THz range.

References

[1] T.C.L.G. Sollner, W.D. Goodhue, P.E. Tannewald, C.D. Parker, and D.D. Peck, Appl. Phys. Letters. **43**, 588 (1983).

[2] E.R. Brown, J.R. Soderstrom, C.D. Parker, J.J. Mahoney, K.M. Molvar, and T.C. McGill, Appl. Phys. Lett. **58**, 2291 (1991).

[3] E.R. Brown, in *Heterostructures and Quantum Devices,* edited by N.G. Einspruch and W.R. Frensley (Academic, Orlando, 1993), Chap. 10, p. 305.

[4] F.A. Buot and K.L. Jensen, Int. J. Comp. Math. Electr. Electron. Eng., **COMPEL 10**, 241 (1991).

[5] D.L. Woolard, E.R. Brown, F.A. Buot, X.J. Lu, D.L. Rhodes, and B.S. Perlman, in *53rd Annual Device Research Conference Digest*, p. 54, 1995.

[6] C.Y. Belhadj, K.P. Martin, S. Ben Amor, J.J.L. Rascol, R.C. Potter, H. Hier, and E. Hempfling, Appl. Phys. Lett. **57**, 58 (1990).

[7] H.C. Liu, Appl. Phys. Lett. **53**, 485 (1988).

[8] C. Kidner, I. Mehdi, J.R. East, and G.I. Haddad, IEEE Trans. Electron Devices **ED-38**, 864 (1990).

[9] K.L. Jensen and F.A. Buot, Phys. Rev. Lett. **66**, 1078 (1991).

[10] V.J. Goldman, D.C. Tsui, and J.E. Cunningham, Phys. Rev. Lett. **58**, 1256, (1987).

[11] T.C.L.G. Sollner, Phys. Rev. Lett. **59**, 1622 (1987)

[12] K.L. Jensen and F.A. Buot, IEEE Trans. Electron Devices **ED-38**, 2337 (1991).

[13] F.A. Buot and K.L. Jensen, Phys. Rev. **B 42**, 9429 (1990).

[14] F.A. Buot and A.K. Rajagopal, Phys. Rev. **B 48**, 17 217 (1993).

[15] R. Landauer and T. Martin, Rev. Mod. Phys. **66**, 217 (1994).

[16] W.R. Frensley, Rev. Mod. Phys. **62**, 765 (1990).

[17] N.C. Kluksdahl, A.M. Kriman, D.K. Ferry, and C. Ringhofer, IEEE Trans. Electron Device Lett. **EDL-9**, 457 (1988).

[18] E.R. Brown, C.D. Parker, and T.C.L.G. Sollner, Appl. Phys. Lett. **54**, 934 (1989).

[19] F.A. Buot and A.K. Rajagopal, Appl. Phys. Lett. **64**, 2994 (1994); **65** 3153 (1994).

[20] F.W. Sheard and G.A. Toombs, Appl. Phys. Lett. **52**, 1228 (1988).

[21] F.A. Buot and A.K. Rajagopal, J. Appl. Phys. **76**, 5552 (1994).

[22] A. Zaslavsky, V.J. Goldman, D.C. Tsui, and J.E. Cunningham, Appl. Phys. Lett. **53**, 1408 (1988).

[23] E.S. Alves, L. Eaves, M. Henini, O.H. Hughes, M.L. Leadbeater, F.W. Sheard, G.A. Toombs, G. Hill, and M.A. Pate, Electron. Lett. **24**, 1190 (1988).

[24] L.O. Chua, C.A. Desoer, and E.S. Kuh, *Linear and Nonlinear Circuits* (McGraw-Hill, New York, 1987).

[25] D.L. Woolard, F.A. Buot, D.L. Rhodes, X.J. Lu, and B.S. Perlman, (unpublished).

[26] A. Grub, A. Simon, H.L. Hartnagel, J. Brune, M. Raum, and H. Brand in *Proceedings of the Sixth International Symposium on Space Terahertz Technology*, p. 8, 1995.

[27] L. Brand, *Differential and Difference Equations* (Wiley, New York, 1966).

[28] T.B. Bahder, C.A. Morrison, and J.D. Bruno, Appl. Phys. Lett. **51**, 1089 (1987).

ARMY RESEARCH LABORATORY
PHYSICAL SCIENCES DIRECTORATE
MANDATORY DISTRIBUTION LIST

Defense Technical Information Center*
ATTN: DTIC-OCC
8725 John J. Kingman Rd STE 0944
Fort Belvoir, VA 22060-6218
(*Note: Two DTIC copies will be sent from STINFO office, Ft. Monmouth, NJ)

Director
US Army Material Systems Analysis Actv
ATTN: DRXSY-MP
(1) Aberdeen Proving Ground, MD 21005

Commander, AMC
ATTN: AMCDE-SC
5001 Eisenhower Ave.
(1) Alexandria, VA 22333-0001

Director
Army Research Laboratory
ATTN: AMSRL-D (John W. Lyons)
2800 Powder Mill Road
(1) Adelphi, MD 20783-1197

Director
Army Research Laboratory
ATTN: AMSRL-DD (COL Thomas A. Dunn)
2800 Powder Mill Road
(1) Adelphi, MD 20783-1197

Director
Army Research Laboratory
2800 Powder Mill Road
Adelphi, MD 20783-1197
(1) AMSRL-OP-SD-TA (ARL Records Mgt)
(1) AMSRL-OP-SD-TL (ARL Tech Library)
(1) AMSRL-OP-SD-TP (ARL Tech Publ Br)

Directorate Executive
Army Research Laboratory
Physical Sciences Directorate
Fort Monmouth, NJ 07703-5601
(1) AMSRL-PS-A (V. Rosati)
(1) AMSRL-PS-T (M. Hayes)
(22) Originating Office

Advisory Group on Electron Devices
ATTN: Documents
Crystal Square 4
1745 Jefferson Davis Highway, Suite 500
(2) Arlington, VA 22202

Commander, CECOM
R&D Technical Library
Fort Monmouth, NJ 07703-5703
(1) AMSEL-IM-BM-I-L-R (Tech Library)
(3) AMSEL-IM-BM-I-L-R (STINFO Ofc)

ARMY RESEARCH LABORATORY
PHYSICAL SCIENCES DIRECTORATE
SUPPLEMENTAL DISTRIBUTION LIST
(ELECTIVE)

Deputy for Science & Technology
Office, Asst Sec Army (R&D)
(1) Washington, DC 20310

HQDA (DAMA-ARZ-D/
Dr. F.D. Verderame)
(1) Washington, DC 20310

Director
Naval Research Laboratory
ATTN: Code 2627
(1) Washington, DC 20375-5000

USAF Rome Laboratory
Technical Library, FL2810
ATTN: Documents Library
Corridor W, STE 262, RL/SUL
26 Electronics Parkway, Bldg. 106
Griffiss Air Force Base
(1) NY 13441-4514

Dir, ARL Battlefield
Environment Directorate
ATTN: AMSRL-BE
White Sands Missile Range
(1) NM 88002-5501

Dir, ARL Sensors, Signatures,
Signal & Information Processing
Directorate (S3I)
ATTN: AMSRL-SS
2800 Powder Mill Road
(1) Adelphi, MD 20783-1197

Dir, CECOM Night Vision/
Electronic Sensors Directorate
ATTN: AMSEL-RD-NV-D
(1) Fort Belvoir, VA 22060-5806

Dir, CECOM Intelligence and
Electronic Warfare Directorate
ATTN: AMSEL-RD-IEW-D
Vint Hill Farms Station
(1) Warrenton, VA 22186-5100

Cdr. Marine Corps Liaison Office
ATTN: AMSEL-LN-MC
(1) Fort Monmouth, NJ 07703-5033